

Post-fission properties of uranium isotopes: a hybrid method with Langevin dynamics and the Hauser-Feshbach statistical model

S. Tanaka (田中翔也)^{1,*}, N. Nishimura (西村信哉)^{2,1,†}, F. Minato (湊太志)^{3,1,‡} and Y. Aritomo (有友嘉浩)^{4,§}

¹*RIKEN Nishina Center for Accelerator-Based Science, Wako, Saitama 351-0198, Japan*

²*Astrophysical Big Bang Laboratory, RIKEN, Wako, Saitama 351-0198, Japan*

³*Department of Physics, Kyushu University, Fukuoka 819-0395, Japan*

⁴*Faculty of Science and Engineering, Kindai University, Higashi-Osaka, Osaka 577-8502, Japan*

(Dated: July 19, 2023)

Background: Precise understanding of nuclear fission is crucial for experimental and theoretical nuclear physics, astrophysics, and industrial applications; however, the complete physical mechanics is unresolved due to the complexities. **Purpose:** In this study, we present a new method to describe the dynamical-fission process and following prompt-neutron emission, where we combine the dynamical fission calculation based on the Langevin method and the Hauser-Feshbach statistical model. **Methods:** Two methods are connected smoothly within the universal charge distribution and the energy conservation, allowing us to calculate a sequence of fission dynamics and post-fission phase, including prompt neutron emission. **Results:** Using a certain set of model parameters, we successfully reproduce the experimental primary-fission yields, total kinetic energy, independent-fission yields, and prompt neutron emissions for the neutron induced fission of ^{236}U , a compound nucleus of $n + ^{235}\text{U}$. We elucidate the physical mechanism of the characteristic features observed in previous experiments, such as shell properties. Additionally, we apply our calculation to two very neutron-rich uranium isotopes, i.e., ^{250}U and ^{255}U , which are not experimentally confirmed but are important for r-process nucleosynthesis. Theoretical results indicate that ^{250}U exhibits an asymmetric multiple-peak fission yield distribution, while the neutron-rich ^{255}U has a single peak due to symmetric fission. Our method predicts post-neutron emission fragments, where ^{250}U shows a stronger neutron emissivity than ^{255}U . **Conclusions:** Our framework is highly reproducible in the experiments and shows that the number of emitted neutrons after fission differs significantly in neutron-rich uranium fission depending on distributions of fission variables.

I. INTRODUCTION

Nuclear fission is a decay process in which a heavier nucleus is split into two or lighter nuclei, usually occurring in actinide elements (e.g., uranium) and further heavier nuclei [1, 2]. Fission can also be interpreted as the production process of unstable nuclei and nuclear-excited states, which may be accompanied by additional radioactive decay such as γ -ray decay and particle emission (e.g., neutrons and α particles). It is thus essential to understand the entire process, including the nuclear states of fission fragments involved in fission and subsequent particle emissions. A quantitative understanding of nuclear fission is crucial for nuclear engineering, but it is also an interesting subject in fundamental physics, such as nuclear physics and astrophysics. The fission of neutron-rich nuclei is of particularly importance in understanding the physics of unstable nuclei and its application to r-process nucleosynthesis, which occurs in neutron-rich astrophysical environments, e.g., in compact-object-binary mergers [3–6] (and see recent reviews, e.g., [7–9]).

The fission process begins with the dynamical behaviour of unstable or excited nuclei, which are more

challenging to be described within a theoretical model than a single nucleus in a stable state. Its study requires us to track the entire time evolution of a nucleus until it splits into multiple nuclei. Therefore, a full understanding of fission dynamics within ab-initio approaches is still quite a difficult task. Many microscopic approaches based on energy density functionals have been examined [10–19], providing us plenty of knowledge to improve descriptions of fission dynamics. However, they are still not capable of reproducing experimental data of total kinetic energies (TKEs) and fragment yields simultaneously. Another approach to describe the fission process is the phenomenological method based on a fluctuation-dissipation method by Langevin equations [20–24], in which the dynamics are described by the motion of *classical* droplets, including quantum effects (such as nuclear-shell structure) as the nuclear potential. The method has successfully reproduced experimental values, including fission fragments and TKEs with appropriate physical parameters, and has been used not only in the field of applied nuclear physics but also in the research of the fundamental physics of unstable nuclei as a robust way to describe fission properties.

Fission is, however, a complex process where various phases are involved even after separations into multifragments. The primary-fission-product nuclei, which are usually in excited states, immediately undertake several decay processes, e.g., neutron emissions and radiative decays. The decay properties of actinides were measured

* shoya.tanaka@riken.jp

† nobuya.nishimura@riken.jp

‡ minato.futoshi@phys.kyushu-u.ac.jp

§ aritomo@ele.kindai.ac.jp

precisely because of their critical importance in applications such as nuclear reactors. However, such a post-fission process has not been considered in previous dynamical calculations and has yet to be compared with experimental data. Recently, the accuracy of TKEs and fission fragment yields calculated within the Langevin equation significantly improved, opening a new possibility to study radiative decays and fission dynamics comprehensively.

It is necessary to follow the post-fission process precisely to explain experimental data on a wide variety of fission. The post-fission stage involves different physics from dynamical fission, so we must adopt other physical descriptions and models in addition to the Langevin approaches. To deal with particle evaporation from the post-fission stage, the Hauser-Feshbach statistical model (HFSM) is one of the appropriate methods in which fission fragments are assumed to reach a thermal equilibrium immediately. The HFSM has already been applied to prompt neutron emissions for neutron- and photo-induced fission of actinide nuclei [25–29] as well as β -delayed neutron emissions [30, 31]. Comparison of theoretical calculations to various experiments enables to constrain and refine the adopted parameters in the Langevin model and HFSM.

In this study, we quantitatively investigate nuclear decay processes that occur subsequently to dynamical fission. The primary objective is to establish a calculation method that exhibits higher experimental reproducibility, particularly for significant physical phenomena such as neutron emissions. To this end, we incorporate the Langevin calculation (the Kindai University Langevin model: KiLM) for fission dynamics and the HFSM for post-neutron emission (implemented in CCONE [32]). By utilizing the hybrid method that connects the dynamical Langevin model and HFSM calculations, we successfully reproduce experimental fission data. To study the performance of our framework, a neutron-induced reaction on ^{236}U is chosen. We also extend the framework to neutron-rich uranium isotopes of ^{250}U and ^{255}U , which have not been experimentally evaluated.

The paper is structured as follows. Section II describes nuclear models and numerical methods for fission calculations and the post-fission process. The results of ^{236}U and neutron-rich isotopes are shown in Section III. Section IV is devoted to summary and conclusions.

II. METHODS

To calculate the fission dynamics and the subsequent decay process of daughter nuclei, we employ a hybrid approach that combines the dynamical Langevin scheme and the HFSM. Our calculation scheme involves modeling a sequence of dynamical fission phases followed by post-fission neutron emissions. Fig. 1 shows a schematic picture of the fission process and prompt neutron emission that we investigate in this study. The following sec-

tions describe the calculation methods used in individual phases, including the physical parameter setups.

A. The dynamical fission calculation

To calculate nuclear-shape time evolution, we use the fluctuation-dissipation model with Langevin equation, the Kindai University Langevin model (KiLM) [39–41]. The nuclear shape is defined by the two-center parametrization [42, 43], which has three deformation parameters, z , δ and α to serve as collective coordinates, abbreviated as $q = \{z, \delta, \alpha\}$. The symbol z is the distance between two potential centers, the symbol δ denotes the deformation of the fragments, and $\alpha = (A_1 - A_2)/(A_1 + A_2)$ is the mass asymmetry of the two fragments [39], where A_1 and A_2 denote the mass numbers of heavy and light fragments.

For a given value of the temperature of a system T which is related with the excitation energy of the composite system as $E^* = aT^2$ (a is the level density parameter [20, 44]), the potential energy is defined as a sum of the liquid-drop (LD) part and a microscopic (SH) part:

$$\begin{aligned} V(q, T) &= V_{\text{LD}}(q) + V_{\text{SH}}(q, T), \\ V_{\text{LD}}(q) &= E_{\text{S}}(q) + E_{\text{C}}(q), \\ V_{\text{SH}}(q, T) &= [\Delta E_{\text{shell}}(q) + \Delta E_{\text{pair}}(q)]\Phi(T), \quad (1) \\ \Phi(T) &= \exp\left(-\frac{aT^2}{E_d}\right). \end{aligned}$$

Here, the potential energy V_{LD} is calculated with the finite-range liquid drop model [45], given as a sum of the surface energy E_{S} and the Coulomb energy E_{C} . The microscopic energy V_{SH} at $T = 0$ is calculated as the sum of the shell correction energy ΔE_{shell} , evaluated by the Strutinsky method [46, 47], and the pairing correlation correction energy ΔE_{pair} [46, 48]. The shell correction energy has a temperature dependence expressed by a factor $\Phi(T)$ in which the shell damping energy E_d is chosen as 20 MeV [49]. We assume that the angular momentum of fissioning nucleus is not large at the low excitation energy, so the rotational energy is not included in Eqs. (1).

To define the potential of the two-center shell model [42, 43], a neck parameter of $\varepsilon = 0.35$ ($0 \leq \varepsilon \leq 1$) [50] has been routinely used [20, 40, 51–54]. However, this value is not appropriate for heavier actinide nuclides as pointed out in [53, 55]. We adopt the optimal ε values following the empirical relation

$$\varepsilon(A_c) = 0.01007A_c - 1.94, \quad (2)$$

where A_c is the mass of the fissioning nucleus.

The multi-dimensional Langevin equations (see, e.g.,

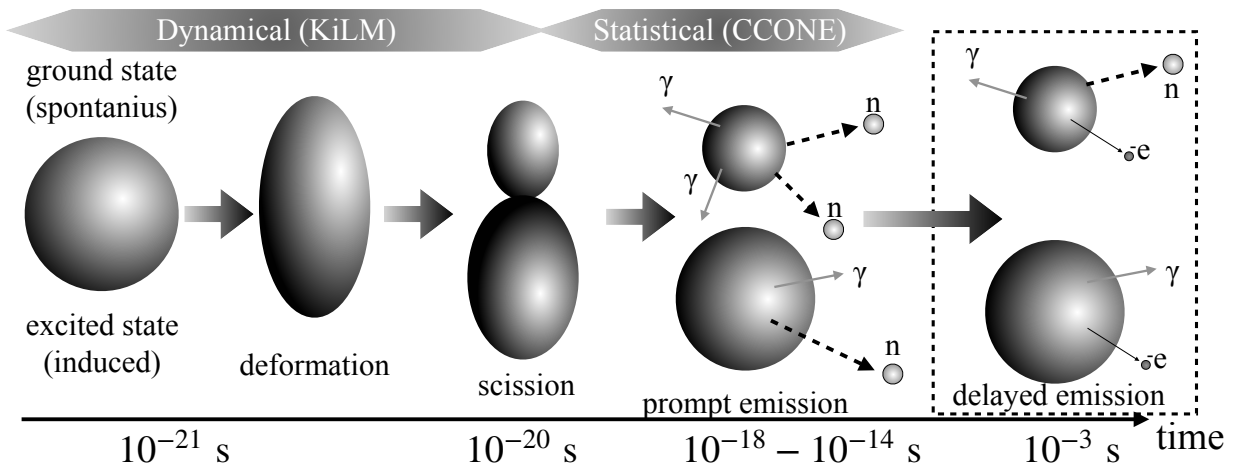


FIG. 1. Schematic representation of fission dynamics and the following prompt-neutron emission process (followed by delayed emission and decay). The change of nuclear shape splitting into two nuclei are described with typical time scales. See texts for details of the dynamical model by KiLM (Section II A) and the statistical model by CCONE (Section II C).

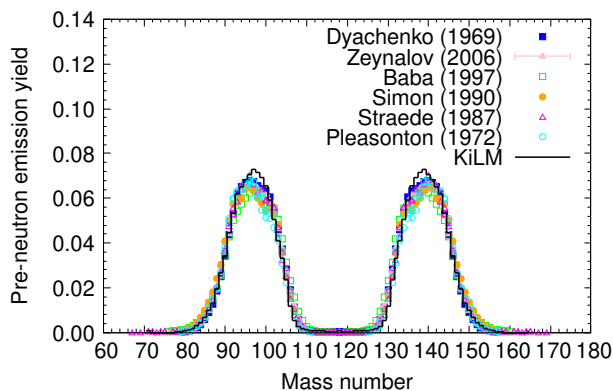


FIG. 2. The normalized fission yields of ^{236}U , which is the compound nucleus of $^{235}\text{U} + n$. The numerical results by KiLM are compared with several experimental data [33–38].

[39]) are given as

$$\begin{aligned} \frac{dq_i}{dt} &= (m^{-1})_{ij} p_j, \\ \frac{dp_i}{dt} &= -\frac{\partial V}{\partial q_i} - \frac{1}{2} \frac{\partial}{\partial q_i} (m^{-1})_{jk} p_j p_k \\ &\quad - \gamma_{ij} (m^{-1})_{jk} p_k + g_{ij} R_j(t), \end{aligned} \quad (3)$$

where $q_i = \{z, \delta, \alpha\}$ and $p_i = m_{ij} dq_i/dt$ is a momentum conjugate to coordinate q_i . In the Langevin equation, m_{ij} and γ_{ij} are the shape-dependent collective inertia and the friction tensors, respectively. The wall-and-window one-body dissipation [56–58] is adopted for the friction tensor.

The normalized random force $R_i(t)$ is assumed to be that of white noise, i.e.,

$$\begin{aligned} \langle R_i(t) \rangle &= 0, \\ \langle R_i(t_1) R_j(t_2) \rangle &= 2\delta_{ij} \delta(t_1 - t_2). \end{aligned} \quad (4)$$

The strength of the random force g_{ij} is related to the friction tensor γ_{ij} by the classical Einstein relation [59],

$$\begin{aligned} \sum_k g_{ik} g_{jk} &= \gamma_{ij} T^*, \\ T^* &= \frac{\hbar\omega}{2} \coth\left(\frac{\hbar\omega}{2T}\right), \end{aligned} \quad (5)$$

where T^* is the effective temperature [60]. The parameter ω is the local frequency of collective motion [59]. The minimum of T^* is given by $\hbar\omega/2$, which corresponds to zero-point energy of oscillators forming the heat bath. We estimated the zero-point energy as 3.05 MeV to be consistent with experimental data, which is higher than the previous study.

The random properties introduced in Eqs. (3)–(5) give different trajectories on the potential energy space event-by-event, creating the fission fragment mass distribution by accumulating enough number of different trajectories, which can be directly compared to the experimental data. In each trajectory, fission is defined as the case that nucleus reaches the scission point on the potential energy surface. The calculation result for fission fragment mass distribution of ^{236}U ($E^* = 9$ MeV) is shown in Fig. 2 with several experimental data, where the mass distribution is reasonably reproduced. This excitation energy is adopted for numerical efficiency, which may be a relatively higher than experiments. However, it is a lower value than ones adopted in previous Langevin calculations [20, 40].

B. The unchanged-charge distribution and total kinetic energy (TKE)

Since the dynamical fission calculations with the KiLM consider the mass of each nucleus but does not the atomic

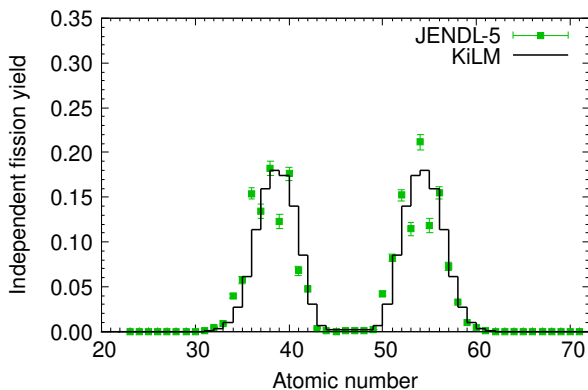


FIG. 3. The normalized fission yield distribution of ^{236}U against the atomic number (the charge distribution), based on the UCD. The results of the KiLM are compared with the evaluated data of JENDL-5 [61].

number (Z), we assume the *unchanged-charge distribution* (UCD) hypothesis to estimate fission fragment charge distributions. The UCD assumption is a simple treatment; the most probable charge of a fission fragment Z_f is determined from the ratio of atomic number to mass of parent nuclei, i.e., $Z_f = A_f Z_{\text{CN}} / A_{\text{CN}}$, where A_{CN} and Z_{CN} are mass and atomic number of compound nucleus, and A_f is the fragment mass, respectively.

Experimental data show that charge distribution of fission fragments slightly deviates from the UCD [62, 63]; however, it is not easy to estimate the deviations for neutron-rich nuclei, where no experimental data are available. We therefore use the UCD assumption mentioned above to estimate charge distributions in our calculations. Fortunately, the deviations from UCD do not significantly affect prompt neutron yields. However, we need to pay attention to the charge distribution more seriously if delayed neutron yields are discussed as pointed out in Refs. [27, 64]. We would like to mention one theoretical approach that has calculated charge fragmentation of ^{240}Pu within a Hartree-Fock-Bogoliubov + particle number projection [65], which has a potential to predict charge distributions of unmeasured fissioning nuclei.

To consider the charge polarization, the fragment charge number Z_1 is randomly determined by following a Gaussian distribution based on the UCD assumption in KiLM, where the mean value μ_{Z_1} is set to

$$\mu_{Z_1} = \frac{Z_{\text{CN}}}{A_{\text{CN}}} A_1 - 0.5 \quad (6)$$

with the standard deviation of $\sigma = 0.493$, a typical value of the charge distribution [63, 66]. The Z_2 is automatically determined by $Z_2 = Z_{\text{CN}} - Z_1$. The calculated charge distribution of ^{236}U ($E^* = 9$ MeV) is shown in Fig. 3. Although an odd-even staggering is observed in the evaluated data of charge distribution of $n_{\text{th}} + ^{235}\text{U}$ [61], our calculation reasonably reproduces the distribution.

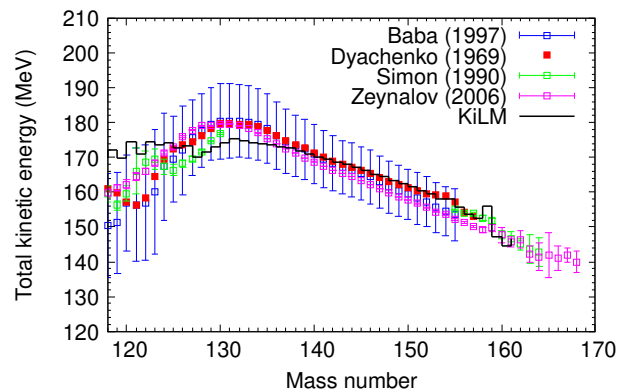


FIG. 4. The mean value of the TKE for ^{236}U . The results by KiLM are compared with experimental data [33–36].

The TKE of fission fragments is assumed to be given by

$$\text{TKE} = V_{\text{Coul}} + E_{\text{pre}}, \quad (7)$$

where $V_{\text{Coul}} = Z_1 Z_2 e^2 / D$ and E_{pre} are the Coulomb repulsion energy of point charges of fragments and the pre-scission kinetic energy. The distance between centers of mass of the left and right parts of the nucleus at the scission point is represented by D . The pre-scission kinetic energy E_{pre} is given by

$$E_{\text{pre}} = \frac{1}{2} (m^{-1})_{ij} p_i p_j, \quad (8)$$

which is calculated at the scission point. The statistical average of E_{pre} of ^{236}U ($E^* = 9$ MeV) in the KiLM is equal to 5.93 MeV. Therefore, the main contribution to the TKE comes from the Coulomb repulsion of fission fragments. The mean value of the TKE ($\langle \text{TKE} \rangle$) as a function of the fission fragment mass is shown in Fig. 4 for the fission of ^{236}U at $E^* = 9$ MeV. Averaging over fission mass yields, we obtain $\langle \text{TKE} \rangle = 170.16$ MeV. The KiLM overestimates the $\langle \text{TKE} \rangle$ around $A = 120$ and underestimates around $A = 130$. On the other hand, it reproduces well for $A \geq 136$. We expect the deviations of $\langle \text{TKE} \rangle$ from $A = 120$ to 136 does not affect too much prompt-neutron emissions because the fragment mass yields are much smaller than $A \geq 136$ as seen in Fig. 2.

C. The Hauser-Feshbach statistical model

We use the HFSM with width-fluctuation correction implemented in CCONE code [32] to estimate particle evaporation from excited fission fragments at the post fission evolution, including the prompt neutron emission. To carry out the HFSM calculation, excitation energy and spin-parity distributions of fragments defined as $\rho(J^\pi, E^*) = \rho(J^\pi) \rho(E^*)$ are needed. The energy partition between light and heavy fragments are determined

by an anisothermal parameter R_T defined by [67]

$$R_T = \frac{T_l}{T_h} = \sqrt{\frac{a_h(U_h)U_l}{a_l(U_l)U_h}}, \quad (9)$$

where $a_{l,h}$ is the energy-dependent level density parameter and $U_{l,h}$ is the energy corrected by the pairing energy Δ , $U_{l,h} = E_{l,h} - \Delta_{l,h}$. The excitation energy $E_{l,h}$ are determined in an iterative way from Eq. (9). Here we define the total excitation energy (TXE) as

$$\text{TXE} = E_l + E_h = M_C - (M_l + M_h) - \text{TKE} + E^*, \quad (10)$$

where M_C , M_l , and M_h are the mass of compound system, light fragment, and heavy fragment, respectively. We set in this work $R_T = 1.2$ that is determined from the $n+^{235}\text{U}$ reaction [26]. The excitation energy distribution is then calculated by [25–27]

$$\rho(E_{l,h}^*) = \frac{1}{\sqrt{2\pi\delta_{l,h}^2}} \exp\left(-\frac{(E_{l,h}^* - E_{l,h})^2}{2\delta_{l,h}^2}\right), \quad (11)$$

where the width parameter $\delta_{l,h}$ is estimated by

$$\delta_{l,h} = \frac{\delta_{\text{TXE}}}{\sqrt{E_l^2 + E_h^2}} E_{l,h}. \quad (12)$$

The width parameter $\delta_{\text{TXE}} = \delta_{\text{TKE}}$ is calculated from KiLM and UCD described in Sect. II A and II B.

For the spin-parity distribution of fragments, a widely-applied expression:

$$\rho(J^\pi) = \frac{1}{2} \frac{J+1/2}{2(f\sigma(U))^2} \exp\left(-\frac{(J+1/2)^2}{2(f\sigma(U))^2}\right), \quad (13)$$

is used where $\sigma(U)$ is the spin cutoff parameter and we use the same value of $f = 2.756$ as determined from the $n+^{235}\text{U}$ reaction [26].

Transmission coefficients of nucleons are calculated by the optical potentials of Koning-Delaroche [68]. For nuclear level densities, the Gilbert-Cameron method [69] with Mengoni-Nakajima parameter [70] is adopted. For γ strength functions, the enhanced generalized Lorentzian function [71] is used. Mass data are taken from the AME2020 [72].

III. RESULTS

A. Fission properties of ^{236}U

As described in Section II, we calculate the prompt neutron emission process within the HFSSM implemented in CCONE, following the dynamical calculation with the KiLM for the induced fission of ^{236}U , i.e., a compound nucleus of $n + ^{235}\text{U}$ in the present study. The outputs calculated by KiLM for ^{236}U , e.g., the mass distribution of fission yields (Fig. 2), the charge distribution with

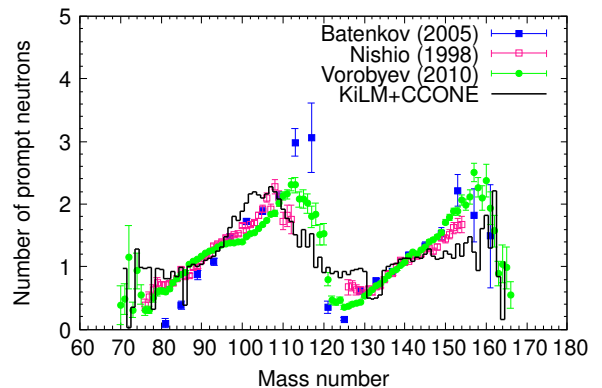


FIG. 5. The number of prompt neutrons for ^{236}U . The calculated values with a solid line (KiLM+CCONE) as a function of the mass number are compared with evaluated data [73–75]. The calculated average neutron emission number is $\langle n \rangle = 2.413$.

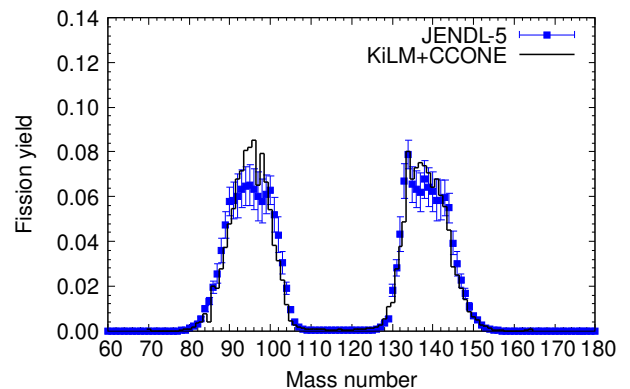


FIG. 6. The normalized fission yields of ^{236}U (the compound nucleus of $^{236}\text{U} + n$) calculated by KiLM+CCONE after the prompt neutron emission is compared with evaluated data (JENDL-5 [61]).

the UCD assumption (Fig. 3), and the TKE distributions (Fig. 4) are collected to carry out the calculation of CCONE.

The numerical results of the number of prompt neutrons as a function of the mass number are shown in Fig. 5. The global trend of experiments, the so-called saw-tooth structure that yields the increase from $A = 70$ (130) to around 110 (160) and the decrease from $A = 110$ (160) to 120 (170), are reproduced feasibly although the position of the peaks deviates from the experimental data. Although the physical origin of the saw-tooth structure is not clarified well, we can qualitatively understand that suppression around $A = 120$ is due to the shell effect of Sn isotopes with $Z = 50$, where its decay and particle emission are weakened. The broad framework is thus characterized by the strong influence of dynamics and shell potentials. Our calculated results are close the most to the experimental data by Nishio (1998) [74] among available experimental data but have discrep-

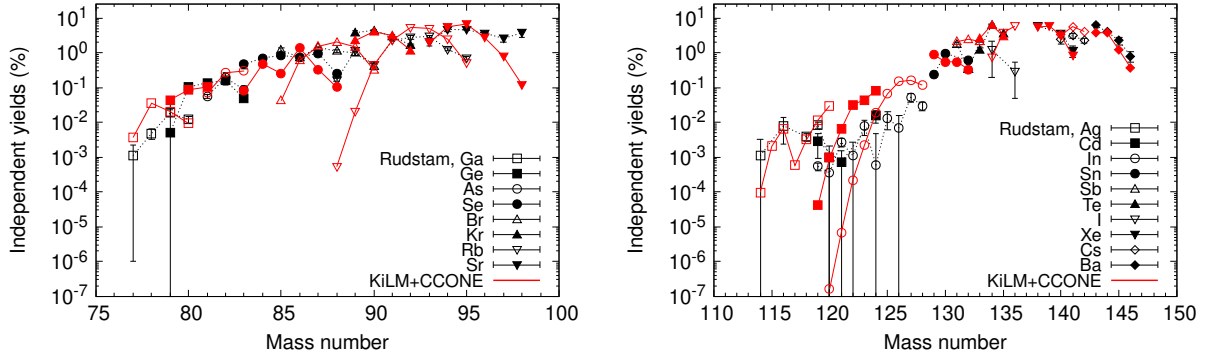


FIG. 7. The independent yields of individual isotopes with experimental data [76]. Experimentally identified isotopes are selected: $^{77-80}\text{Ga}$, $^{79-83}\text{Ge}$, $^{81-83}\text{As}$, $^{83-88}\text{Se}$, $^{85-90}\text{Br}$, $^{89-92}\text{Kr}$, $^{88-95}\text{Rb}$, and $^{93-98}\text{Sr}$ in the left panel and $^{114,116,118-120}\text{Ag}$, $^{119,120,124}\text{Cd}$, $^{119-128}\text{In}$, $^{129,130,132}\text{Sn}$, $^{131-133}\text{Sb}$, $^{133-135}\text{Te}$, $^{134,136}\text{I}$, $^{138,140,141}\text{Xe}$, $^{140-142}\text{Cs}$, and $^{143-146}\text{Ba}$ in the right panel.

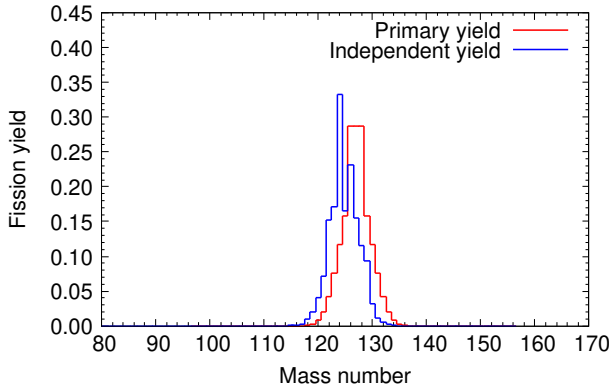
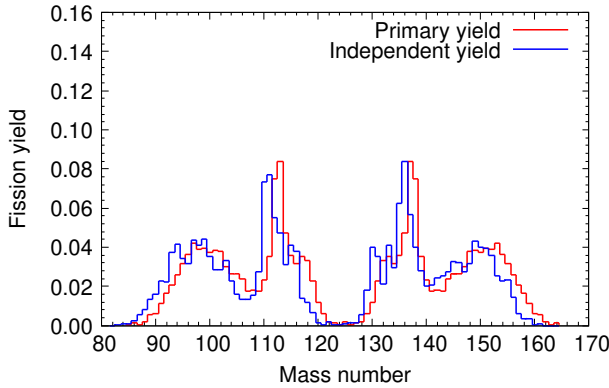


FIG. 8. The normalized distribution of fission yields for ^{250}U (top) and ^{255}U (bottom). The primary yield distribution and the independent fission yields are compared.

ancies with the other two experiments near the lower boundary ($A < 80$) and higher boundary ($A > 150$), as well as a steep drop in the range of $A \sim 110$ to 120 . Because experimental results of those regions still exhibit significant dispersion, further investigation in terms of both experiment and theoretical models must be necessary.

Fig. 6 shows the independent fission yields after

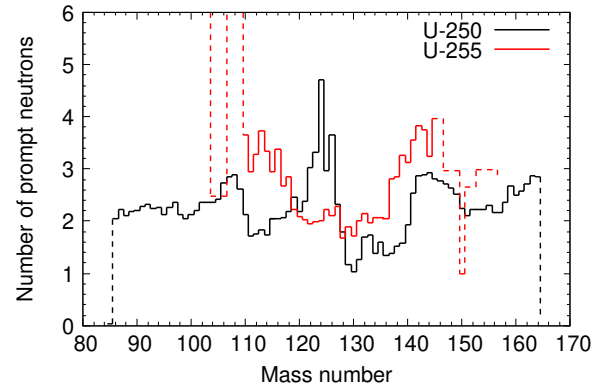


FIG. 9. The number of prompt neutrons as a function of fragment mass for ^{250}U (black line) and ^{255}U (red line). The solid line corresponds the statistically significant range, while the dotted indicate lower statistics influenced by one or few fission events. The average neutron emission numbers are $\langle n \rangle = 4.185$ for ^{250}U and $\langle n \rangle = 3.434$ for ^{255}U .

prompt-neutron emission. The evaluated data by JENDL-5 is compared with our numerical results by the KiLM+CCONE calculation. The distribution represents the independent fission yields after neutron emission from the primary fission shown in Fig. 2. The corresponding fission yield reduces by a few mass units due to few neutron emissions. We can see that heavier fission yields in the range of $A = 130$ to 150 , in particular, exhibit excellent agreement with evaluated data. This indicates the high reproducibility of our fission+neutron emission calculations. On the other hand, while the overall distribution of lighter peaks is well reproduced, there are some discrepancies in areas that exhibit complex structures. Based on the calculation, the average number of the prompt neutrons per one fission event is $\langle n \rangle = 2.574$, which is in good agreement with the evaluated value of $\langle n \rangle = 2.413$ [61]. Although there are some minor discrepancies in the fission yield distribution, the overall features are well reproduced.

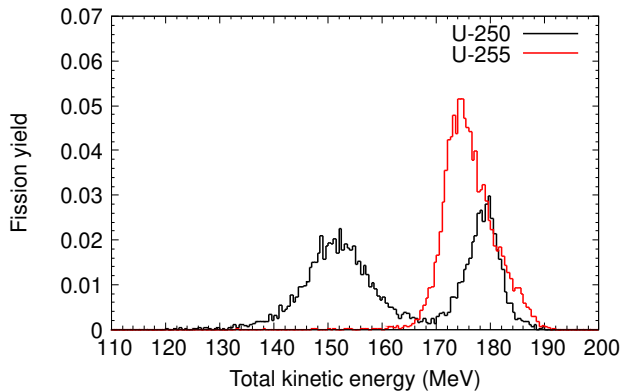


FIG. 10. The fission yield distribution in the TKE for ^{250}U (black line) and ^{255}U (red line). The average TKE values are $\langle \text{TKE} \rangle = 162.50$ MeV for ^{250}U and $\langle \text{TKE} \rangle = 175.85$ MeV for ^{255}U .

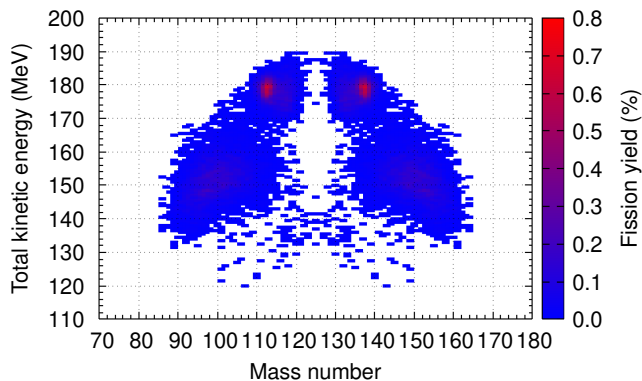


FIG. 11. The fission yield distribution of ^{250}U on the TKE–mass number plane. The color scale indicates fission yields.

Fig. 7 presents the isotopic distributions of fission products, compared with the experimental data [76]. As expected by the high reproducibility of fission yields, our results reproduce experiments well, except for nuclei with large experimental errors or limited statistics in fission yields. This highlights the robustness of our calculations across multiple data sets, including charge distributions. We should note, however, that our dynamics calculations still utilize a simplified charge distribution with the UCD assumption, which may cause some discrepancies. Further investigations with advanced treatment of the charge distribution (e.g., [65, 77]) are still expected to make our framework more sophisticated.

B. Neutron-rich U isotopes: ^{250}U and ^{255}U

Using the KiLM+CCONE method, we calculate nuclear fission and prompt-neutron emissions for two additional neutron-rich U isotopes, ^{250}U and ^{255}U . The calculated primary fission yields before prompt neutron emission and independent fission yields after prompt neutron

emission are shown in Fig. 8. The yields of ^{250}U show four peaks (two strong and moderate double peaks) due to different two mass-asymmetric fission modes, while those of ^{255}U have a single peak by mass-symmetric fission. Our previous dynamical fission calculations also confirm the transition from asymmetric to symmetric fission in neutron-rich U isotopes, the preliminary results of which were reported in Refs. [78, 79]. A similar transition has also been experimentally confirmed in Fm isotopes with mass numbers close to the present study ($^{254,256,258}\text{Fm}$) [80–82]. Fig. 8 shows that the independent fission yields distribute in smaller mass regions than the primary fission due to the prompt neutron emissions. The characteristic point of the independent fission yields is a more detailed distribution than the primary fission yields, which originates from the shell structure of fission fragments. For example, staggering around $A \sim 96, 130$ become prominent for ^{250}U and the independent yields show two peaks at $A = 124$ and 126 for ^{255}U that is not present in the primary yields.

The number of emitted neutrons as a function of fragment mass for ^{250}U and ^{255}U is plotted in Fig. 9. The solid line represents the statistically significant range, while the dotted line may overestimate the average emitted neutrons with tiny fission products, which have negligible impact on the overall discussion. The results of those neutron-rich nuclei are different from ^{236}U in Fig. 5. A significant difference is the disappearance of the saw-tooth structure observed for ^{236}U . Instead, a peak is found in $A \sim 125$ for ^{250}U , and a large number of neutrons is emitted from light fragments and $A \sim 144$ for ^{255}U . Analyzing the calculated results, the peak for ^{250}U and many neutron emissions for ^{255}U resulted from the contributions from many fission fragments rather than those from one or a few specific nuclei. In other words, as discussed in the following paragraph, this is relevant to the excitation energy of fission fragments. Those outstanding peaks do not contribute significantly to the average number of prompt neutrons because the corresponding fission yields are relatively small.

Fig. 10 is the case of ^{250}U , two distinct peaks are seen at $\text{TKE} \sim 150$ MeV and ~ 180 MeV. In contrast, ^{255}U exhibits only a single peak around $\text{TKE} = 175$ MeV. The single peak structure is a natural consequence because ^{255}U does mass-symmetric fission, while two peak structure found in ^{250}U originates from the fact that ^{250}U does asymmetric fission having four peak structure in the mass distributions as seen in Fig. 8. Considering the energy conservation, fragment pairs with a small TKE have a large TXE, while those with a high TKE have a small TXE. Namely, most fission fragments with $A \sim 115$ (135) for the induced-fission of ^{250}U have a rather larger TXE than those for ^{255}U . To explain this, we also plot in Fig. 11 the fission yield distribution of ^{250}U on the TKE–mass number plane. We can identify that $\text{TKE} = 150$ MeV and 180 MeV peaks of ^{250}U correspond to the peak-pairs of $A \sim 115$ (and 135) and $A \sim 95$ (and 150), respectively. Since the Coulomb energies at

the scission point (V_{Coul}), the major contributor to TKE, are different for fragment pairs, two peaks of TKE can be explained by four peak structures in the mass distributions. We can also see that the distribution of TKE around $A \sim 124$ relatively concentrates on smaller TKE around 130–140 MeV, resulting in fission fragments with high excitation energies. As a consequence, we have a sharp peak around $A \sim 124$ for the number of prompt neutrons of ^{250}U in Fig. 9.

For ^{250}U , the emission of prompt neutrons is dominated by nuclei with $A \sim 100$ and 150 in the moderate double peaks. This is because the TKE is relatively low, and the TXE is high. In the case of ^{255}U , which exhibits only the single peak in the mass distribution, neutrons are mainly emitted from nuclei with $A \sim 128$, which have a relatively small number of prompt neutron emissions (Fig. 9) because the TKE is high and the corresponding TXE is expected to be relatively small. The calculated average number of prompt neutrons is $\langle n \rangle = 4.185$ for ^{250}U , which is larger than the case of ^{236}U with $\langle n \rangle = 2.413$ mainly due to lower neutron binding energy. However, the average number of prompt neutrons is $\langle n \rangle = 3.434$ for ^{255}U , which is smaller than ^{250}U . From our calculations, neutron-rich U isotopes, which have not been experimentally identified, may exhibit a higher number of prompt neutrons than fission of nuclei along β -stability line; however, depending on fission modes and TKE distributions, as in case of neutron-rich ^{255}U , the number of prompt neutrons would not monotonically increase with neutron number.

IV. SUMMARY AND CONCLUSIONS

In this study, we calculated the fission properties of uranium isotopes with a newly developed method based on a dynamical fission method (KiLM) and a HFSSM (CCONE). Using a certain set of model parameters, we successfully reproduce experimental fission-fragment distributions, TKE, and prompt neutron emissions for the induced fission of ^{236}U , which is a compound nucleus of $n+^{235}\text{U}$, and two very neutron-rich uranium isotopes, i.e., ^{250}U and ^{255}U , which are not experimentally confirmed, but are relevant to r-process nucleosynthesis. Our results are summarised as follows:

1. We accurately calculated the fission yields and TKE of ^{236}U using the KiLM with appropriate physical parameters, successfully reproducing the experimental values. We applied the same method to the induced fission of ^{250}U and ^{255}U . These results were consistently and smoothly connected to the subsequent HFSSM calculations.
2. The post-neutron emission properties of ^{236}U were explained from the physical point of view, and the experimental data were well reproduced. The average number of prompt neutrons, with a $\langle n \rangle = 2.574$,

was in excellent agreement with the experimental value.

3. We performed neutron emission calculations of very neutron-rich uranium isotopes where experimental data is unavailable. In the case of asymmetric fission, ^{250}U , we obtained $\langle n \rangle = 4.185$, while the mass-symmetric fission of ^{255}U we had $\langle n \rangle = 3.434$. From these results, we concluded that the number of prompt neutrons does not necessarily increase with neutron number, and it is important to understand fission mode and TKE distributions.

Our novel calculation method, combining the Langevin and HFSSM approaches, has successfully reproduced experimental data for ^{236}U , including fission products and TKE. The remaining discrepancies can potentially be resolved by refining the model used in dynamical calculations, particularly in cases where experimental evaluations have lower accuracy. We can improve reproducibility by reducing symmetry in the nuclear shape parameters. Future advancements, building upon the findings of this study, hold the potential for enhancing our understanding of the underlying physics. Since there are other nuclei besides ^{236}U for which neutron emission has been measured, it will be intriguing to extend the application to other nuclei for future research.

Even in the absence of experimental data for neutron-rich nuclei, i.e., ^{250}U and ^{255}U , various quantities related to fission and neutron emission can be predicted with fundamental physical validity. This region represents the transition from mass-asymmetric fission to symmetric fission as the mass number increases with neutron excess. In the range of asymmetric fission, where there is an excess of neutrons, the number of emitted neutrons tends to increase. Conversely, in the range of symmetric fission, the neutron excess tends to decrease, resulting in a decrease in the number of emitted neutrons. This behaviour can be understood by examining the distribution of TKE.

In future, improving the reproducibility of experimental data will be crucial, along with the systematic development of highly accurate theoretical predictions. Understanding the nature of fission, especially in neutron-rich nuclei, is vital for applications in r-process nucleosynthesis occurring in space. The study of fission effects in neutron-rich nuclei heavily relies on theoretical approaches, which have primarily focused on half-life and fission distribution systematics. However, the results obtained from dynamical models have yet to be fully utilized in practical applications. It is important to continue investigating the effects of symmetric fission in neutron-rich nuclei and their associated neutron emission numbers, as suggested in this study, to advance our understanding of r-process nucleosynthesis.

ACKNOWLEDGMENTS

The authors thank O. Iwamoto for his support for using the CCONE code. The also authors acknowledge helpful discussion with participants at “RIBF-ULIC-

miniWS038,” funded by RIBF ULOR at RIKEN. Parts of the computations shown in the present study were carried out on computer facilities on CfCA at NAOJ and YITP at Kyoto University. The project was financially supported by JSPS KAKENHI (19H00693, 20H05648, 21H01087, 21H01856, 22K20373). N.N. was supported by the RIKEN Incentive Research Projects.

-
- [1] O. Hahn and F. Strassmann. Über den Nachweis und das Verhalten der bei der Bestrahlung des Urans mittels Neutronen entstehenden Erdalkalimetalle. *Naturwissenschaften*, 27(1):11–15, January 1939.
- [2] Lise Meitner and O. R. Frisch. Disintegration of Uranium by Neutrons: a New Type of Nuclear Reaction. *Nature (London)*, 143(3615):239–240, February 1939.
- [3] M. Eichler, A. Arcones, A. Kelic, O. Korobkin, K. Langanke, T. Marketin, G. Martinez-Pinedo, I. Panov, T. Rauscher, S. Rosswog, C. Winteler, N. T. Zinner, and F. K. Thielemann. The Role of Fission in Neutron Star Mergers and Its Impact on the r-Process Peaks. *Astrophys. J.*, 808(1):30, July 2015.
- [4] Y. Zhu, R. T. Wollaeger, N. Vassh, R. Surman, T. M. Sprouse, and others. Californium-254 and Kilonova Light Curves. *Astro. Phys. J. Lett.*, 863(2):L23, August 2018.
- [5] J. F. Lemaître, S. Goriely, A. Bauswein, and H. T. Janka. Fission fragment distributions and their impact on the r-process nucleosynthesis in neutron star mergers. *Phys. Rev. C*, 103(2):025806, February 2021.
- [6] Shinya Wanajo, Sho Fujibayashi, Kota Hayashi, Kenta Kiuchi, Yuichiro Sekiguchi, and Masaru Shibata. Actinide-boosting r Process in Black Hole-Neutron Star Merger Ejecta. *arXiv e-prints*, page arXiv:2212.04507, December 2022.
- [7] M. Arnould and S. Goriely. Astronuclear Physics: A tale of the atomic nuclei in the skies. *Progress in Particle and Nuclear Physics*, 112:103766, May 2020.
- [8] John J. Cowan, Christopher Sneden, James E. Lawler, Ani Aprahamian, Michael Wiescher, Karlheinz Langanke, Gabriel Martínez-Pinedo, and Friedrich-Karl Thielemann. Origin of the heaviest elements: The rapid neutron-capture process. *Reviews of Modern Physics*, 93(1):015002, January 2021.
- [9] H. Schatz, A. D. Becerril Reyes, A. Best, E. F. Brown, K. Chatziioannou, and others. Horizons: nuclear astrophysics in the 2020s and beyond. *Journal of Physics G Nuclear Physics*, 49(11):110502, November 2022.
- [10] Michael Bender, Rémi Bernard, George Bertsch, Satoshi Chiba, Jacek Dobaczewski, Noël Dubray, et al. Future of nuclear fission theory. *Journal of Physics G: Nuclear and Particle Physics*, 47(11):113002, oct 2020.
- [11] N. Schunck, M. Verriere, G. Potel Aguilar, R. C. Malone, J. A. Silano, A. P. D. Ramirez, and A. P. Tonchev. Microscopic calculation of fission product yields for odd-mass nuclei. *Phys. Rev. C*, 107:044312, Apr 2023.
- [12] Z. X. Ren, J. Zhao, D. Vretenar, T. Nikšić, P. W. Zhao, and J. Meng. Microscopic analysis of induced nuclear fission dynamics. *Phys. Rev. C*, 105:044313, Apr 2022.
- [13] Jie Zhao, Tamara Nikšić, and Dario Vretenar. Time-dependent generator coordinate method study of fission: Dissipation effects. *Phys. Rev. C*, 105:054604, May 2022.
- [14] Jie Zhao, Tamara Nikšić, and Dario Vretenar. Time-dependent generator coordinate method study of fission. ii. total kinetic energy distribution. *Phys. Rev. C*, 106:054609, Nov 2022.
- [15] R. Rodríguez-Guzmán, Y.M. Humadi, and L.M. Robledo. Microscopic description of fission in superheavy nuclei with the parametrization d1m* of the gogny energy density functional. *Eur. Phys. J. A*, 56:43, Feb 2020.
- [16] A. Taninah, S. E. Agbemava, and A. V. Afanasjev. Covariant density functional theory input for r-process simulations in actinides and superheavy nuclei: The ground state and fission properties. *Phys. Rev. C*, 102:054330, Nov 2020.
- [17] Aurel Bulgac. Angular correlation between the fission fragment intrinsic spins. *Phys. Rev. C*, 106:014624, Jul 2022.
- [18] Jhilam Sadhukhan, Samuel A. Giuliani, and Witold Nazarewicz. Theoretical description of fission yields: Toward a fast and efficient global model. *Phys. Rev. C*, 105:014619, Jan 2022.
- [19] Yu Qiang, J. C. Pei, and P. D. Stevenson. Fission dynamics of compound nuclei: Pairing versus fluctuations. *Phys. Rev. C*, 103:L031304, Mar 2021.
- [20] Y. Aritomo, S. Chiba, and F. Ivanyuk. Fission dynamics at low excitation energy. *Phys. Rev. C*, 90(5):054609, November 2014.
- [21] S. Tanaka, Y. Aritomo, Y. Miyamoto, K. Hirose, and K. Nishio. Effects of multichance fission on isotope dependence of fission fragment mass distributions at high energies. *Phys. Rev. C*, 100:064605, Dec 2019.
- [22] R. Léguillon, K. Nishio, K. Hirose, H. Makii, I. Nishinaka, R. Orlandi, K. Tsukada, J. Smallcombe, S. Chiba, Y. Aritomo, T. Ohtsuki, R. Tatsuzawa, N. Takaki, N. Tamura, S. Goto, I. Tsekhanovich, C.M. Petrache, and A.N. Andreyev. Fission fragments mass distributions of nuclei populated by the multinucleon transfer channels of the $18\text{o}+232\text{th}$ reaction. *Physics Letters B*, 761:125–130, 2016.
- [23] K. Hirose, K. Nishio, S. Tanaka, R. Léguillon, H. Makii, I. Nishinaka, R. Orlandi, K. Tsukada, J. Smallcombe, M. J. Vermeulen, S. Chiba, Y. Aritomo, T. Ohtsuki, K. Nakano, S. Araki, Y. Watanabe, R. Tatsuzawa, N. Takaki, N. Tamura, S. Goto, I. Tsekhanovich, and A. N. Andreyev. Role of multichance fission in the description of fission-fragment mass distributions at high energies. *Phys. Rev. Lett.*, 119:222501, Nov 2017.
- [24] M. J. Vermeulen, K. Nishio, K. Hirose, K. R. Kean, H. Makii, R. Orlandi, K. Tsukada, I. Tsekhanovich, A. N. Andreyev, S. Ishizaki, M. Okubayashi, S. Tanaka, and Y. Aritomo. Measurement of fission-fragment mass distributions in the multinucleon transfer channels of the $^{18}\text{O} + ^{237}\text{Np}$ reaction. *Phys. Rev. C*, 102:054610, Nov

- 2020.
- [25] Shin Okumura, Toshihiko Kawano, Patrick Jaffke, Patrick Talou, and Satoshi Chiba. $^{235}\text{U}(n,f)$ independent fission product yield and isomeric ratio calculated with the statistical hauser-feshbach theory. *Journal of Nuclear Science and Technology*, 55(9):1009–1023, 2018.
- [26] A. E. Lovell, T. Kawano, S. Okumura, I. Stetcu, M. R. Mumpower, and P. Talou. Extension of the hauser-feshbach fission fragment decay model to multichance fission. *Phys. Rev. C*, 103:014615, Jan 2021.
- [27] Shin Okumura, Toshihiko Kawano, Amy Elizabeth Lovell, and Tadashi Yoshida. Energy dependent calculations of fission product, prompt, and delayed neutron yields for neutron induced fission on ^{235}U , ^{238}U , and ^{239}Pu . *J. of Nucl. Sci. Technol.*, 59:96–109, 2021.
- [28] H. Almazán, L. Bernard, A. Blanchet, A. Bonhomme, C. Buck, A. Chalil, A. Chebboubi, P. del Amo Sanchez, I. El Atmani, L. Labit, J. Lamblin, A. Letourneau, D. Lhuillier, M. Licciardi, M. Lindner, O. Litaize, T. Matera, H. Pessard, J.-S. Réal, J.-S. Ricol, C. Roca, R. Rogly, T. Salagnac, V. Savu, S. Schoppmann, T. Soldner, A. Stutz, L. Thulliez, and M. Vialat. Improved fifeilin de-excitation model for neutrino applications. *The European Physical Journal A*, 59:75, 2023.
- [29] T. Kawano, A. E. Lovell, S. Okumura, H. Sasaki, I. Stetcu, and P. Talou. Consideration of memory of spin and parity in the fissioning compound nucleus by applying the hauser-feshbach fission fragment decay model to photonuclear reactions. *Phys. Rev. C*, 107:044608, Apr 2023.
- [30] Futoshi Minato, Tomislav Marketin, and Nils Paar. β -delayed neutron-emission and fission calculations within relativistic quasiparticle random-phase approximation and a statistical model. *Phys. Rev. C*, 104:044321, Oct 2021.
- [31] M. R. Mumpower, T. Kawano, and T. M. Sprouse. β^- -delayed fission in the coupled quasiparticle random-phase approximation plus hauser-feshbach approach. *Phys. Rev. C*, 106:065805, Dec 2022.
- [32] O. Iwamoto, N. Iwamoto, S. Kunieda, F. Minato, and K. Shibata. The CCONe Code System and its Application to Nuclear Data Evaluation for Fission and Other Reactions. *Nuclear Data Sheets*, 131:259–288, January 2016.
- [33] PP Dyachenko, BD Kuzminov, and MZ Tarasko. Energy and mass distributions of fragments from fission of ^{235}U by monoenergetic neutrons from 0-meV to 15.5-meV. *Soviet Journal of Nuclear Physics-USSR*, 8(2):165–+, 1969.
- [34] S. Zeynalov, V. Furman, F.-J. Hamsch, M. Florec, V. Yu. Konovalov, V. A. Khryachkov, and Yu. S. Zamyatnin, 2006. Joint Institute for Nuclear Research, Russia.
- [35] Hiroshi BABA, Tadashi SAITO, Naruto TAKAHASHI, Akihiko YOKOYAMA, Takahiro MIYAUCHI, Sige-hisa MORI, Daisaku YANO, Teruyuki HAKODA, Koichi TAKAMIYA, Kiyoshi NAKANISHI, and Yoshihiro NAKAGOME. Role of effective distance in the fission mechanism study by the double-energy measurement for uranium isotopes. *Journal of Nuclear Science and Technology*, 34(9):871–881, 1997.
- [36] G. Simon, J. Trochon, F. Brisard, and C. Signarbieux. Pulse height defect in an ionization chamber investigated by cold fission measurements. *Nuclear Instruments and Methods in Physics Research Section A: Accelerators, Spectrometers, Detectors and Associated Equip-ment*, 286(1):220–229, 1990.
- [37] Ch. Straede, C. Budtz-Jørgensen, and H.-H. Knitter. $^{235}\text{U}(n, f)$ fragment mass-, kinetic energy- and angular distributions for incident neutron energies between thermal and 6 meV. *Nuclear Physics A*, 462(1):85–108, 1987.
- [38] Frances Pleasonton, Robert L. Ferguson, and H. W. Schmitt. Prompt gamma rays emitted in the thermal-neutron-induced fission of ^{235}U . *Phys. Rev. C*, 6:1023–1039, Sep 1972.
- [39] Yoshihiro Aritomo and Masahisa Ohta. Dynamical calculation for fusion-fission probability in superheavy mass region, where mass symmetric fission events originate. *Nucl. Phys. A*, 744:3–14, November 2004.
- [40] Y. Aritomo and S. Chiba. Fission process of nuclei at low excitation energies with a Langevin approach. *Phys. Rev. C*, 88(4):044614, October 2013.
- [41] Y. Aritomo, A. Iwamoto, K. Nishio, and M. Ohta. Fission mechanism inferred from nuclear shape fluctuation by the Langevin equation. *Phys. Rev. C*, 105(3):034604, March 2022.
- [42] Joachim Maruhn and Walter Greiner. The asymmetry two center shell model. *Zeitschrift für Physik*, 251(5):431–457, October 1972.
- [43] K. Sato, A. Iwamoto, K. Harada, S. Yamaji, and S. Yoshida. Microscopic calculation of friction in heavy ion reaction using linear response theory. *Zeitschrift für Physik A Hadrons and Nuclei*, 288(4):383–390, December 1978.
- [44] J. Töke and W. J. Świątecki. Surface-layer corrections to the level-density formula for a diffuse Fermi gas. *Nucl. Phys. A*, 372(1):141–150, December 1981.
- [45] H. J. Krappe, J. R. Nix, and A. J. Sierk. Unified nuclear potential for heavy-ion elastic scattering, fusion, fission, and ground-state masses and deformations. *Phys. Rev. C*, 20(3):992–1013, September 1979.
- [46] V. M. Strutinsky. Shell effects in nuclear masses and deformation energies. *Nucl. Phys. A*, 95(2):420–442, April 1967.
- [47] V. M. Strutinsky. “Shells” in deformed nuclei. *Nucl. Phys. A*, 122(1):1–33, December 1968.
- [48] Sven Gösta Nilsson, Chin Fu Tsang, Adam Sobczewski, Zdzislaw Szymański, Sławomir Wycech, Christer Gustafson, Inger-Lena Lamm, Peter Möller, and Björn Nilsson. On the nuclear structure and stability of heavy and superheavy elements. *Nucl. Phys. A*, 131(1):1–66, January 1969.
- [49] AV Ignatyuk, MG Itkis, VN Okolovich, GN Smirenkin, and AS Tishin. Fission of pre-actinide nuclei. excitation functions for the (α, f) reaction. *Yadernaya Fizika*, 21(6):1185–1205, 1975.
- [50] Shuhei Yamaji, H. Hofmann, and R. Samhammer. Self-consistent transport coefficients for average collective motion at moderately high temperatures. *Nucl. Phys. A*, 475(3):487–518, December 1987.
- [51] R. Léguillon, K. Nishio, K. Hirose, H. Makii, I. Nishinaka, and others. Fission fragments mass distributions of nuclei populated by the multinucleon transfer channels of the $^{18}\text{O} + ^{232}\text{Th}$ reaction. *Physics Letters B*, 761:125–130, October 2016.
- [52] M. D. Usang, F. A. Ivanyuk, C. Ishizuka, and S. Chiba. Effects of microscopic transport coefficients on fission observables calculated by the Langevin equation. *Phys. Rev. C*, 94(4):044602, October 2016.
- [53] K. Hirose, K. Nishio, S. Tanaka, R. Léguillon, H. Makii,

- and others. Role of Multichance Fission in the Description of Fission-Fragment Mass Distributions at High Energies. *Phys. Rev. Lett.*, 119(22):222501, December 2017.
- [54] M. D. Usang, F. A. Ivanyuk, C. Ishizuka, and S. Chiba. Analysis of the total kinetic energy of fission fragments with the Langevin equation. *Phys. Rev. C*, 96(6):064617, December 2017.
- [55] Y. Miyamoto, Y. Aritomo, S. Tanaka, K. Hirose, and K. Nishio. Origin of the dramatic change of fission mode in fermium isotopes investigated using Langevin equations. *Phys. Rev. C*, 99(5):051601, May 2019.
- [56] J. Blocki, Y. Boneh, J. R. Nix, J. Randrup, M. Robel, A. J. Sierk, and W. J. Swiatecki. One-body dissipation and the super-viscosity of nuclei. *Annals of Physics*, 113(2):330–386, August 1978.
- [57] J. Rayford Nix and Arnold J. Sierk. Dynamics of fission and heavy ion reactions. *Nucl. Phys. A*, 428:161–175, October 1984.
- [58] H. Feldmeier. REVIEW ARTICLE: Transport phenomena in dissipative heavy-ion collisions: the one-body dissipation approach. *Reports on Progress in Physics*, 50(8):915–994, August 1987.
- [59] H. Hofmann and D. Kiderlen. A self-consistent treatment of damped motion for stable and unstable collective modes. *International Journal of Modern Physics E*, 07(02):243–274, 1998.
- [60] Chikako Ishizuka, Mark D. Usang, Fedir A. Ivanyuk, Joachim A. Maruhn, Katsuhisa Nishio, and Satoshi Chiba. Four-dimensional langevin approach to low-energy nuclear fission of ^{236}U . *Phys. Rev. C*, 96:064616, Dec 2017.
- [61] Osamu Iwamoto, Nobuyuki Iwamoto, Satoshi Kunieda, Futoshi Minato, Shinsuke Nakayama, Yutaka Abe, Kohsuke Tsubakihara, Shin Okumura, Chikako Ishizuka, Tadashi Yoshida, Satoshi Chiba, Naohiko Otuka, Jean-Christophe Sublet, Hiroki Iwamoto, Kazuyoshi Yamamoto, Yasunobu Nagaya, Kenichi Tada, Chikara Konno, Norihiro Matsuda, Kenji Yokoyama, Hiroshi Tanihara, Akito Oizumi, Masahiro Fukushima, Shoichiro Okita, Go Chiba, Satoshi Sato, Masayuki Ohta, and Saerom Kwon. Japanese evaluated nuclear data library version 5: Jendl-5. *Journal of Nuclear Science and Technology*, 60(1):1–60, 2023.
- [62] A.C. Wahl. Systematics of fission-product yields. Technical report, Los Alamos National Laboratory, 2022. LA-13928.
- [63] T.R. England and B.F. Rider. Evaluation and compilation of fission product yields. Technical report, Los Alamos National Laboratory, 1994. LA-UR-94-3106.
- [64] Futoshi Minato. Neutron energy dependence of delayed neutron yields and its assessments. *Journal of Nuclear Science and Technology*, 55(9):1054–1064, 2018.
- [65] Marc Verriere, Nicolas Schunck, and Toshihiko Kawano. Number of particles in fission fragments. *Phys. Rev. C*, 100:024612, Aug 2019.
- [66] Arthur C. Wahl. Nuclear-charge distribution and delayed-neutron yields for thermal-neutron-induced fission of ^{235}u , ^{233}u , and ^{239}pu and for spontaneous fission of ^{252}cf . *Atomic Data and Nuclear Data Tables*, 39(1):1–156, 1988.
- [67] T. Kawano, P. Talou, I. Stetcu, and M.B. Chadwick. Statistical and evaporation models for the neutron emission energy spectrum in the center-of-mass system from fission fragments. *Nuclear Physics A*, 913:51–70, 2013.
- [68] A.J. Koning and J.P. Delaroche. Local and global nucleon optical models from 1 keV to 200 MeV. *Nuclear Physics*, A713:231, 2003.
- [69] Gilbert A. and Cameron A.G.W. A composite nuclear-level density formula with shell corrections. *Can. J. Phys.*, 43:1446, 1965.
- [70] Mengoni A. and Y. Nakajima. Fermi-gas model parametrization of nuclear level density. *Journal of Nuclear Science Technology*, 31:151–162, 1994.
- [71] J. Kopecky and M. Uhl. Test of gamma-ray strength functions in nuclear reaction model calculations. *Phys. Rev. C*, 41:1941–1955, May 1990.
- [72] W.J. Huang, Meng Wang, F.G. Kondev, G. Audi, and S. Naimi. The AME 2020 atomic mass evaluation (i). evaluation of input data, and adjustment procedures*. *Chinese Physics C*, 45(3):030002, mar 2021.
- [73] O. A. Batenkov, G. A. Boykov, F. J. Habsch, J. H. Hamilton, V. A. Jakovlev, V. A. Kalinin, A. B. Laptev, V. E. Sokolov, and A. S. Vorobyev. Prompt Neutron Emission in the Neutron-Induced Fission of ^{239}Pu and ^{235}U . *AIP Conf. Proc.*, 769(1):1003, 2005.
- [74] K. Nishio, Y. Nakagome, H. Yamamoto, and I. Kimura. Multiplicity and energy of neutrons from $^{235}\text{u}(\text{n},\text{f})$ fission fragments. *Nuclear Physics A*, 632(4):540–558, 1998.
- [75] A. S. Vorobyev, O. A. Shcherbakov, A. M. Gagarin, G. V. Val'Ski, and G. A. Petrov. Investigation of the prompt neutron emission mechanism in low energy fission of $^{235,233}\text{U}(\text{n},\text{f})$ and $^{252}\text{Cf}(\text{sf})$. In *European Physical Journal Web of Conferences*, volume 8 of *European Physical Journal Web of Conferences*, page 03004, October 2010.
- [76] G. Rudstam, P. I. Johansson, O. Tengblad, P. Aagaard, and J. Eriksen. Beta and Gamma Spectra of Short-Lived Fission Products. *Atomic Data and Nuclear Data Tables*, 45:239, January 1990.
- [77] Shuichiro Ebata, Shin Okumura, Chikako Ishizuka, and Satoshi Chiba. Charge polarization calculated with a microscopic model for the fission fragments of U-236. In *European Physical Journal Web of Conferences*, volume 284 of *European Physical Journal Web of Conferences*, page 04008, July 2023.
- [78] M. Okubayashi, S. Tanaka, Y. Aritomo, S. Ishizaki, S. Amano, and N. Nishimura. Fission fragment distributions of neutron-rich nuclei based on Langevin calculations: toward r-process simulations. *arXiv e-prints*, page arXiv:2105.09272, May 2021.
- [79] Shoya Tanaka, Nobuya Nishimura, Itoshi Nishimura, and Yoshihiro Aritomo. The evaluation of the fission mode and fragment yields of neutron-rich nuclei by the dynamical model. In *European Physical Journal Web of Conferences*, volume 279 of *European Physical Journal Web of Conferences*, page 11021, September 2023.
- [80] J. E. Gindler, K. F. Flynn, L. E. Glendenin, and R. K. Sjoblom. Distribution of mass, kinetic energy, and neutron yield in the spontaneous fission of ^{254}Fm . *Phys. Rev. C*, 16:1483–1492, Oct 1977.
- [81] K. F. Flynn, E. P. Horwitz, C. A. A. Bloomquist, R. F. Barnes, R. K. Sjoblom, P. R. Fields, and L. E. Glendenin. Distribution of mass in the spontaneous fission of ^{256}Fm . *Phys. Rev. C*, 5:1725–1729, May 1972.
- [82] E. K. Hulet, J. F. Wild, R. J. Dougan, R. W. Loughheed, J. H. Landrum, A. D. Dougan, P. A. Baisden, C. M. Henderson, R. J. Dupzyk, R. L. Hahn, M. Schädel, K. Sümmerer, and G. R. Bethune. Spontaneous fission

properties of ^{258}Fm , ^{259}Md , ^{260}Md , ^{258}No , and ^{260}No]: Bi-

modal fission. *Phys. Rev. C*, 40:770–784, Aug 1989.